



HAL
open science

Statistical Prediction of Bone Microstructure Degradation to Study Patient Dependency in Osteoporosis

Seyedfarzad Famouri, Mostafa Baghani, Azadeh Sheidaei, Daniel George, Maryam Mazraehei Farahani, Masoud Shariat Panahi, Majid Baniassadi

► **To cite this version:**

Seyedfarzad Famouri, Mostafa Baghani, Azadeh Sheidaei, Daniel George, Maryam Mazraehei Farahani, et al.. Statistical Prediction of Bone Microstructure Degradation to Study Patient Dependency in Osteoporosis. *Mathematics and Mechanics of Solids*, 2022, 10.1177/10812865221098777. hal-03797745

HAL Id: hal-03797745

<https://hal.science/hal-03797745v1>

Submitted on 4 Oct 2022

HAL is a multi-disciplinary open access archive for the deposit and dissemination of scientific research documents, whether they are published or not. The documents may come from teaching and research institutions in France or abroad, or from public or private research centers.

L'archive ouverte pluridisciplinaire **HAL**, est destinée au dépôt et à la diffusion de documents scientifiques de niveau recherche, publiés ou non, émanant des établissements d'enseignement et de recherche français ou étrangers, des laboratoires publics ou privés.

Statistical Prediction of Bone Microstructure Degradation to Study Patient Dependency in Osteoporosis

Seyedfarzad Famouri ^{1,5}, Mostafa Baghani ¹, Azadeh Sheidaei ², Daniel George ^{3**},
Maryam Mazraehei Farahani ⁴, Masoud Shariat Panahi ¹, Majid Baniassadi ^{1*}

¹ School of Mechanical Engineering, College of Engineering, University of Tehran, Tehran, Iran

² Aerospace Engineering Department, Iowa State University, Ames, IA 50011, United States

³ University of Strasbourg, CNRS, ICube Laboratory, Strasbourg, France

⁴ Tehran University of Medical Sciences, Tehran, Islamic Republic of Iran

⁵ The Robotic Surgery Lab., Mechanical Engineering Dept., Concordia University, Montreal, QC, Canada

Corresponding authors:

* School of Mechanical Engineering, College of Engineering, University of Tehran, Tehran, Iran - m.baniassadi@ut.ac.ir

** University of Strasbourg, CNRS, ICUBE, 67400 Illkirch-Graffenstaden, France - george@unistra.fr

Abstract

Numerical prediction of osteoporosis evolution is a challenging objective in medicine, particularly when one desires to account for patient dependency. The use of statistical methods to reconstruct bone microstructure distribution could be a helpful tool for this prediction, as they are able to provide different types of microstructures that can be optimized to fit with each patient. An initial bone sample was obtained from High-resolution X-ray Computed Tomography (H μ CT). Its microstructure evolution in time using a previously developed degradation model was used as the ground truth. Statistical bone microstructures were reconstructed at different stages of this evolution using two-point correlation functions (TPCF). A blind search approach is used to find the optimized statistical microstructures, and the optimized coefficient showed less than 2% TPCF error between the statistical reconstruction and the degraded model. The statistical models also showed less than 13% error in the corresponding mechanical properties. The results showed a good correlation between the developed approach and the ground truth. The method could be extrapolated to account for the physical characterization of patient dependency to predict bone density loss over time.

Keywords: Osteoporosis, Two-phase recovery, Optimization, Two-Point Correlation Function, bone density prediction

1. Introduction

Bone is a living material constantly renewing itself, resulting in the annual renewal of 25% of trabecular and 3% of cortical bones [1]. Three types of cells, osteoclasts, osteoblasts, and osteocytes are in charge of bone remodeling. It is generally accepted that osteoclasts and osteoblasts, are mainly located on the bone surface. In contrast, osteocytes are located within the solid phase of bone and act as mechanosensors to transmit mechanobiological signals to the osteoblasts and osteoclasts for the bone remodeling to occur [2-8]. For a person suffering from osteoporosis, besides the changes occurring in cancellous bone, cortical bone also becomes more porous; consequently, bones become more fragile and susceptible to fractures [9, 10]. Furthermore, the relationship between the remodeling events, bone's porosity, and mechanical strain energy are determinant of the bone fragility during ageing [11]. Biologically speaking, this bone deterioration is different in cortical and trabecular bones. The amount of volumetric change in mass, density, and volumetric bone mineral density (vBMD) is higher in trabecular bone [12] and it was showed that osteoporotic bone volume fraction loss in trabecular and cortical bone of the femoral neck under the same mechanical load is around 16.5% and 9.4%, respectively [13]. Bone loss is mostly linked to the number and thickness of the bone trabeculae [14], and the loss ratio is a function of age, sex, and type of the bone.

Bone density degradation occurs in everybody with aging, and frequently results in osteoporosis. It originates from an inversion of optimum bone cells activity between osteoblast (that will form the bone) and osteoclasts (that will degrade bone). Above 50 yo, osteoclasts activity becomes higher than osteoblasts in the bone remodeling equilibrium, decreasing overall bone density and leading to osteoporosis evolution. It is therefore important to understand this cell activity equilibrium to study bone density evolution. The interaction between the mechanical load and the biology plays a significant role in this phenomenon. This mechanobiological relation depends on the mechanical behavior of the tissue, gaining stiffness with a minimum amount of material as largely described in the literature, see for example [15-17]. It was studied at multiple length scales starting with the widely known Wolff's law that defines a structural optimization of the bone microstructure as a function of the applied mechanical loads [18, 19], followed by Frost and its Mechanostat proposal [20] linking the mechanical energy to the bone density variation. Bone numerical models are designed based on a phenomenological relation between cells and their microstructure distribution [21]. However, for continuum models, which are widely spread in the literature [22-27], scaling the effect of the material is not often integrated into the structural evolution because of its heterogeneous attributes at the small scales where the classical continuum theory is not able to describe the material behavior correctly [28]. Recently, Giorgio et al. [29] developed a novel method combining the features of Cosserat's and Biot's models that can affect the deformation equilibrium shapes at the macroscopic level. La Valle and Massoumi [30] proposed a new formulation of a nonlinear micropolar model that has been also introduced to measurement the effects of macro-micro relative rotation. Although, at the cellular level, these effects can be important, the Cauchy continuum theory of the material is not realistic any more as described in [31-39] since the cells driving the bone structure evolution are unlikely to be homogeneously distributed. As a result, adequate homogenization methods need to be developed [40-45]. Some numerical models try to predict the bone remodeling kinematics at the trabecular scale, yet they are hardly suitable for long-time evolution, mainly due to the fact that patient dependent bone biology is mainly unknown [46-52]. For this, more detailed coupled mechanical-biological models are required [53-55].

Nowadays, some numerical methods propose to link the bone stiffness and the microstructure distribution [56-60] and comparisons are made between the mechanical properties such as effective stiffness tensor, equivalent stresses, and strain energy distributions for the original and reconstructed models with finite element methods [61, 62]. Famouri et al. [63] applied a new statistical method to generate optimized microstructure models having low volume fractions. In the current work, we used a real bone microstructure as an initial condition, and implement a previously developed degradation model [61] to determine its degradation evolution in time. The generated degraded microstructures are used as ground truth to implement statistical interpolation and optimized reconstruction of intermediate microstructures. The objective is to show the capacity of using statistical tools to reconstruct complex microstructures such as bone in order to extract patients' variability (dependency) through different bone trabecular distributions (various clustering scenarii). We show that the statistical approach of microstructure degradation can correlate well with the ground truth. Part 2 recalls the degradation models to obtain the bone microstructure evolution in time serving as our reference, followed by the statistical method to reconstruct the microstructure at different times of evolution. Part 3 details the results and comparison between the reference model and statistically reconstructed models and Part 4 provides some insight about the usefulness of the proposed method.

2. Method

The real bone sample used in the current work is extracted from [62]. It is used as the initial configuration of bone microstructure from which our previously defined bone degradation model was applied [61]. We used this degradation model to predict osteoporotic bone degradation as a function of time, assuming that it corresponds to the real bone degradation. Hence, it is considered as the ground truth for the follow-up of osteoporotic bone degradation and serves as a comparison point with the statistically reconstructed microstructures.

2.1 Modeling bone degradation

We developed a voxel-based model (as per the imaging technique used to acquire the reference model) to simulate trabecular bone degradation [61]. This model is based on the interaction between bone marrow and trabecular bone. We used this bone degradation model to simulate osteoporotic bone loss. Simulations were performed on a microstructure of bone size of 1 cubic mm. The model was created using the micro-CT of a real bone sample. We hypothesized that degradation starts at the surface of the solid phase of bone, where osteoclasts are primarily present. The amount of bone surface involved in the remodeling equations is related to the surface in contact with the bone marrow at the voxel scale. We used a Particle Swarm Optimization (PSO) optimization algorithm to determine the exchange rate between bone and bone marrow [61] and obtain microstructure evolution as a function of time.

By using statistical functions, the current objective is to reconstruct interpolated bone microstructures at different degradation times. The statistically reconstructed microstructures with the closest mechanical properties and volume fraction compared to the degradation model are optimized through statistical descriptors. The volume fraction of the initial real reference model was 93%. We run the degradation model [61] down to a bone volume fraction of 60%. All statistically reconstructed microstructures with any volume fractions in this range are achievable. For the sake of simplicity, we decide to show results only for a limited number of densities; specifically, models with 84, 73, and 63

% volume fractions were derived. We then compare the statistically reconstructed models with the degraded microstructures obtained from [61].

The original experimental bone microstructure and the final degraded microstructure obtained from the degradation model [61] are shown in Figure 1 together with their mid-thickness cross-sections. These initial and degraded microstructures will define the ground truth against which the statistical reconstruction will be compared.

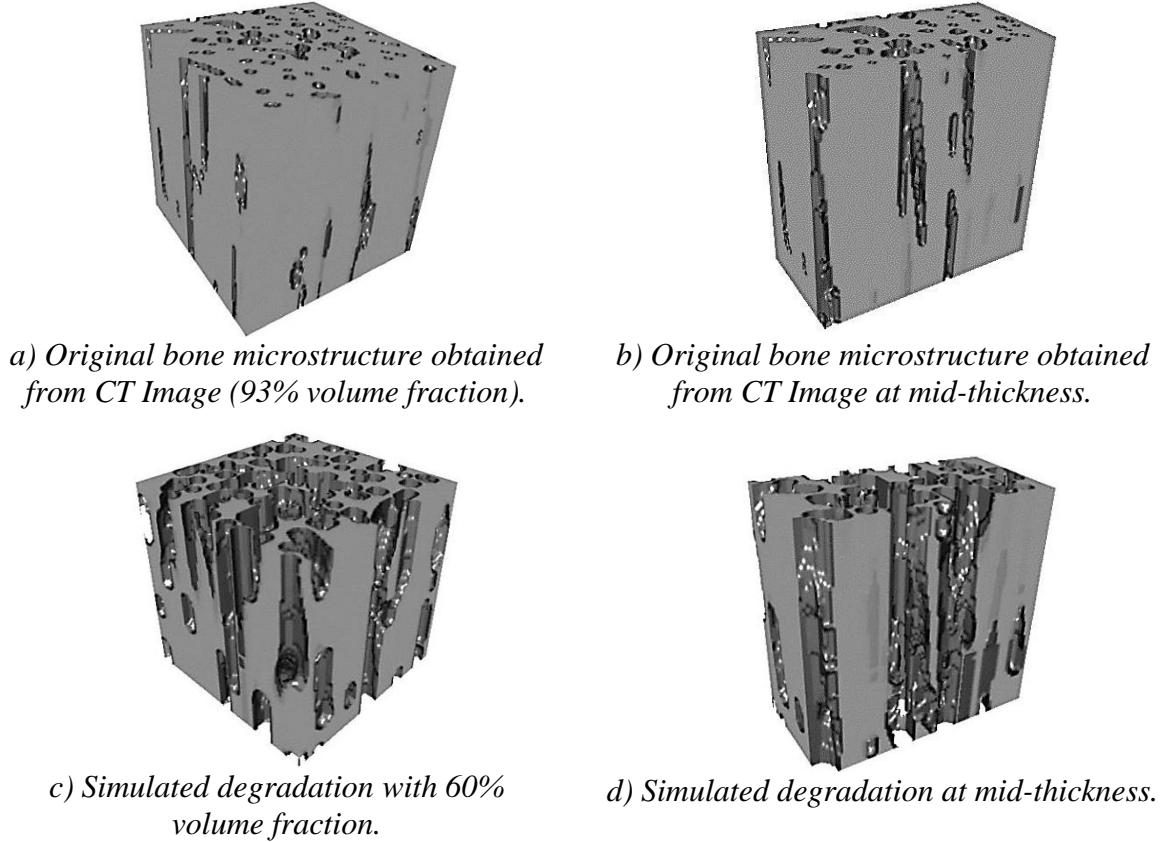


Figure 1: Bone microstructure distribution before and after degradation from [61].

2.2 Statistical interpolation

2.2.1 Theory and definition

N-point correlation functions are used to describe multiphase material's microstructure; for a multiphase material, the microstructure function is defined as:

$$x_p^q = \begin{cases} 1 & \text{if } p \text{ is inside phase } q \\ 0 & \text{otherwise} \end{cases} \quad (1)$$

Here q is the phase and p is the position vector $p = (p_x, p_y, p_z)$. In this investigation, the media is a digitized three-dimensional cubic microstructure with a dimension of $1 \times 1 \times 1$ mm. In the two-phase model, the phases are named q and q' and the grid point is a number between 0 and $p-1$. By considering Eq. (1), one point-correlation function for phase q is defined as:

$$c_1^q = \langle x_p^q \rangle = \frac{1}{Max(p_x).Max(p_y).Max(p_z)} \sum_{p=0}^{p_{max}-1} x_p^q \quad (2)$$

Note that the ensemble is averaged, which means that the asymptotic value for the above function is equivalent to the corresponding volume fraction for each phase and $p_{max} = (Max(p_x), Max(p_y), Max(p_z))$, where Max is the maximum value. Besides, it was shown that a one-point correlation function could be taken to find the upper and lower bound properties of heterogeneous microstructure [64]. The two-point correlation function (an example is provided in Figure 2) is defined below as:

$$c_2^{qq'}(s) = \frac{1}{Max(p_x).Max(p_y).Max(p_z)} \sum_{p=0}^{p_{max}-1} x_p^q x_{p+s}^{q'} \quad (3)$$

It is the first order of geometrical specifications of a microstructure. $s = (s_x, s_y, s_z)$ is the vector for which the TPCF is calculated. Note that TPCF is defined as the relative difference between the voxels' position vectors since grid points in macroscopic homogeneous media are not absolute.

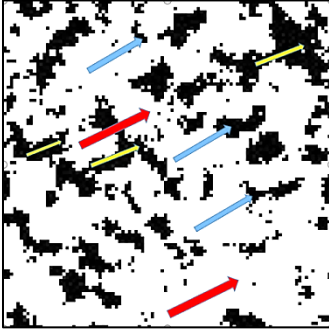


Figure 2: Representation of Two-Point Correlation Functions (TPCF) for a two-phase bone microstructure. Red arrows' head and tails are located in white phase. Yellow arrows are in the black phase. The blue arrows' heads are in the black and tails are in white phase.

TPCFs in a two-phase model are $c_2^{qq}, c_2^{qq'}, c_2^{q'q}$ and $c_2^{q'q'}$ with the following relations :

$$c_2^{qq} + c_2^{qq'} + c_2^{q'q} + c_2^{q'q'} = 1 \quad (4)$$

$$c_2^{qq'} = c_2^{q'q} \quad (5)$$

$$c_2^{qq} + c_2^{q'q'} = v_q \quad (6)$$

v_n is the volume fraction of phase q and is a constant; hence, there is only one independent TPCF for any two-phase microstructure. Other limit constraints for any arbitrary phases like m and n are found in [65] as:

$$\lim_{s \rightarrow 0} c_2^{nm}(s) = \begin{cases} v_n & \text{if } n=m \\ 0 & \text{if } n \neq m \end{cases}, n, m \in \{q, q'\} \quad (7)$$

$$\lim_{s \rightarrow \infty} c_2^{nm}(s) = \begin{cases} v_n^2 & \text{if } n = m \\ v_n v_m & \text{if } n \neq m \end{cases}, n, m \in \{q, q'\} \quad (8)$$

These known limits (from [65]) exist for the values of the two-point correlation functions as s approaches zero or infinity. Note that these limits are general and must be obeyed for random as well as

non-random (including periodic) microstructures. When it comes to calculating TPCF, one way is to use the Fast Fourier Transform (FFT) [66, 67] of the microstructure given by

$$X_k^q = FFT(x_p^q) = \sum_{p=0}^{p_{max}-1} x_p^q e^{[2i\pi(\frac{p_x.k_1}{Max(p_x)} + \frac{p_y.k_2}{Max(p_y)} + \frac{p_z.k_3}{Max(p_z)})]} = |X_k^q| e^{i\theta_k^q} \quad (9)$$

Where $|X_k^q|$ is the amplitude, θ_k^q is the phase of the Fourier transform, and $k = (k_1, k_2, k_3)$ is the Fourier variable.

Another way to obtain the TPCF directly is to use the equation below from [67].

$$FFT(c_2^{qq'}(p)) = \frac{1}{Max(p_x).Max(p_y).Max(p_z)} |X_k^q| e^{i\theta_k^q} |X_k^{q'}| e^{-i\theta_k^{q'}} \quad (10)$$

Finally, when $q=q'$, the equation between FFT of the TPCF and the microstructure function could be found so the TPCFs for every microstructure can be calculated with:

$$FFT(c_2^{qq}(p)) = \frac{1}{Max(p_x).Max(p_y).Max(p_z)} |X_k^q|^2 \quad (11)$$

Next, we used a phase recovery method to predict the microstructure evolution at different times due to the density variation of the solid and non-solid bone microstructure phases. Using TPCF for representing the bone microstructure makes this feasible by using an auto-covariance function as defined in Eq. (12), which is defined for the vector s . It is a linear and scaled function for TPCF, ranging between 0 and 1 when s varies between $s=0$ and $s=\infty$, in order.

$$f_2^q(s) = \frac{c_2^{qq}(s) - v_q^2}{v_q(1 - v_q)} \quad (12)$$

A combination of two or more specific auto-covariance functions as Eq. (12) for different microstructures in different directions enable to obtain a macroscopic homogeneous model (bone microstructure homogenized at the macroscopic scale) to satisfy the essential condition of Eq. (7) and Eq. (8). Thus, new microstructures can be determined using these combinations with new calculated TPCFs.

2.2.2 Microstructure Reconstruction

Producing a microstructure formed on its assigned statistical correlation functions is known as a reconstruction procedure. The inputs for this method are the TPCFs based on Eq. (12) and Eq. (13) below. The phase recovery algorithm (initially used for signal processing [68]) is used in this study based on Eq. (11). By inserting a set of TPCFs into this equation, the amplitudes of the microstructure functions are calculated. The phase recovery is made through using Eq. (9). Hence, the base of the phase recovery algorithm in each cut section reconstruction is defined by Eq. (11). Using the TPCFs of all points of the RVE as input by applying Fast Fourier Series, the x_p^q for all points is calculated.

One of the main difficulties in the proposed objective of microstructure reconstruction is finding the adequate statistical distribution that will be the closest to the real one (in terms of geometrical distribution and mechanical properties). For this, a blind search is developed in order to find optimized coefficients for the statistical reconstruction. It is assumed that f_2^{q1} and f_2^{q2} are two different autocovariance functions that linked to the first and last measurement point (two different times) of

osteoporosis evolution, respectively. Because the sum of the coefficients of two phases should be equal to one to satisfy equations (7) and (8), the auto-covariance of the combined microstructure is :

$$f_2^q(s) = \beta f_2^{q1} + (1 - \beta) f_2^{q2} \quad (13)$$

β is considered a series of discrete values increased by small intervals, yet we are looking for an optimized value, which gives us optimum mechanical properties compared to the degraded microstructure obtained from [61]. It should be noted that Eq. (13) satisfies conditions (7) and (8). β could be any number between 0 and 1. Each number results in a specific TPCF and, consequently, a new bone microstructure model is created.

Using the procedure below, the optimum value of β can be found:

1. Presume β any constant number between 0 and 1
2. Merge the auto-covariance TPCFs from the initial bone microstructure and degraded one so that $f_2^q(s)$ can be calculated.
3. From the inverse of Eq. (12), a new TPCF is found and is used as input data of step 4
4. Reconstruct the model with a two-phase recovery method
5. Find the smallest error between all the iterations compared with the degradation model of [61] explained in paragraph 2.2
6. Finally, the optimum β is found

The steps for the two-phase recovery are shown below in [Figure 3](#).

At the first iteration, a primary random microstructure ($X_{p\ ite}^q$) is generated. The Fast Fourier Transform for this microstructure function is calculated ($X_{k\ ite}^q$) through Eq. (9). Next, the phases of the FFT are preserved, but their modulus ($|X_{p\ ite}^q|$) is replaced with the square root of the $c_{k\ ref}^{qq}$ multiplied by p or $|X_{p\ ref}^q|$ using Eq. (11). The inverse of the Fourier transform of $|X_{k\ ref}^q| e^{i\theta_{k\ ite}^q}$ is taken from the inverse of Eq. (9) and assumed to be the new $X_{p\ ite}^q$ for the next iteration. Then, applying constraints in the real space to the obtained $X_{p\ ite}^q$ by rounding its value, the obtained microstructure in this step is used as an input for the initial iteration back in the loop.

After the last iteration, the error between the TPCFs of the obtained microstructure and $c_{2\ ref}^{qq}$ should be calculated with:

$$Error = \frac{1}{Max(p_x).Max(p_y).Max(p_z)} \sum_{s=0}^{s=p_{max}-1} \frac{|c_{2\ ite}^{qq}(s) - c_{2\ ref}^{qq}(s)|}{c_{2\ ref}^{qq}(s)} \quad (14)$$

If the convergence criteria of error is satisfied, the algorithm will stop and the $X_{p\ ite}^q$ of that step is considered as the final reconstructed microstructure.

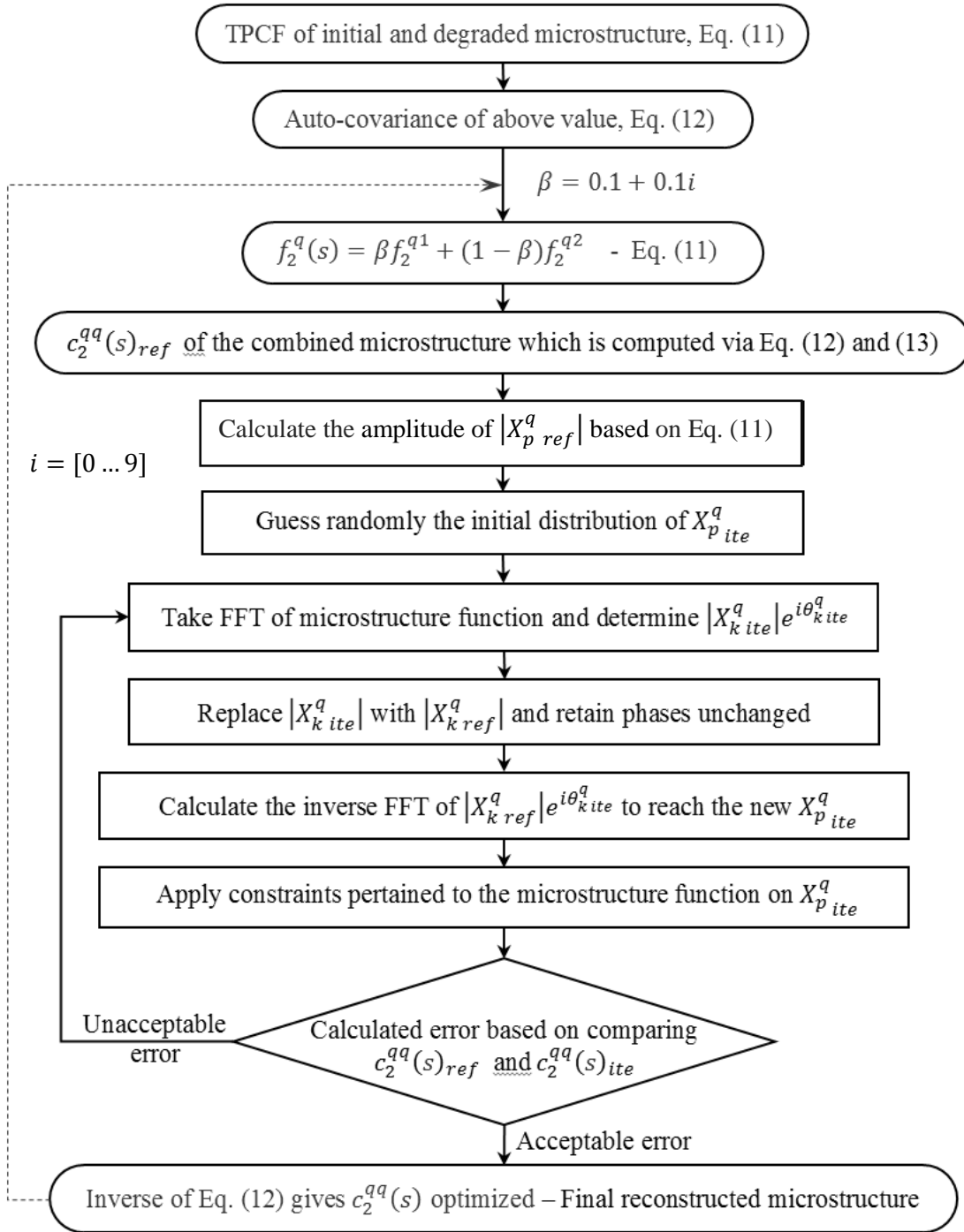


Figure 3: Phase recovery flowchart used for the reconstruction of trabecular bone microstructures

2.3 Effective mechanical properties

For a highly contrasted media like cortical bone, composed of a solid phase with high elastic modulus and a “void” phase with low elastic modulus, the effective properties can be determined easily from the finite element model as described in [61]. We assume that the bone behavior is linear elastic with an effective Young's modulus a function of the bone volume fraction based on Hounsfield scale [61]. It is

supposed to represent a realistic evaluation of a patient's bone strength. Initial and degraded bone samples at different steps were exported to the ABAQUS software to calculate effective elastic modulus. Mechanical loading was applied in the X, Y and Z directions of the bone microstructure and constrained on the opposite face (see Figure 4). Finally, effective mechanical properties were obtained.

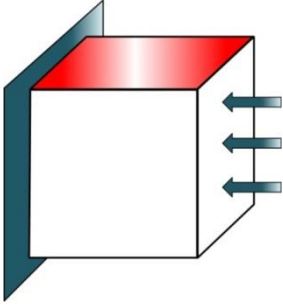


Figure 4: Schematic model of bone sample including forces and boundary conditions for FEM. Constant distributed force is applied on one side where the opposite side is fixed. The three directions x, y, and z are calculated

3. Results

3.1 Interpolation

The TPCFs of the best-reconstructed models for each β are compared with the TPCF of the degradation model generated from [61] with the same volume fraction. The TPCF error between the two cases is given by :

$$Error = \frac{1}{Max(p_x).Max(p_y).Max(p_z)} \sum_{s=0}^{s=p-1} \frac{|c_2^{qq}(s)_{final\ reconstructed\ model} - c_2^{qq}(s)_{numerical\ model}|}{c_2^{qq}(s)_{numerical\ model}} \quad (15)$$

The best β is chosen for each specific volume fraction. Figures 5a to 5c show the comparison between the degraded microstructure (time evolution from [61]) and reconstructed cases (at a given time of evolution from the statistical reconstruction) for the volume fraction of 74%.

The optimized parameter β in Eq. (13) should be chosen between 0 and 1 to satisfy the conditions (7) and (8). The initial value is fixed to be 0.1. After reconstructing the microstructure pertained to the mentioned coefficient, β is increased up to the maximum value of 1 by increment of 0.1. For each reconstructed microstructure, the β parameter is optimized with regard to a minimized error. This is done in turn for each microstructure evolution (time increment). All statistical microstructures matrices are then compared with the degraded model derived from the previous method described in 2-3 [61]. The closest statistical case to the degraded model is chosen. The errors from Eq. (15) are calculated and presented in Table 1 with the optimized β giving the lowest averaged errors for each specific volume fraction.

To better address the quality of the reconstructed microstructures through the precise evaluation of the β parameter and error developed with each of its values, we used 100*100*100 voxel matrix generated from their respective TPCF. We compared the degraded bone from [61] and statistical reconstruction for 63% volume fraction. Their voxel formations (Figure 6) are obtained using a MATLAB code.

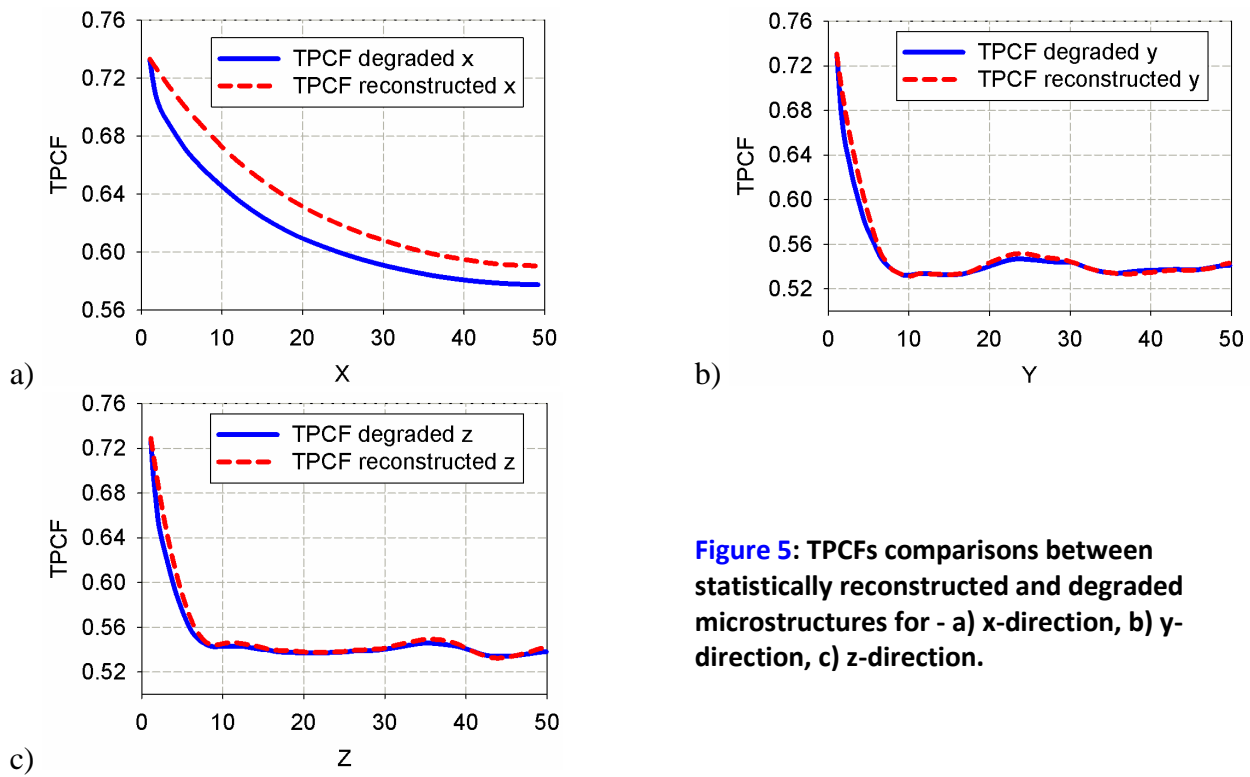


Figure 5: TPCFs comparisons between statistically reconstructed and degraded microstructures for - a) x-direction, b) y-direction, c) z-direction.

Volume Fraction	β	Error (%)
84%	0.5	0.840
73%	0.1	0.204
63%	0.2	1.740

Table 1: Optimized β coefficient for the three volume fractions 84%, 73%, and 63%.

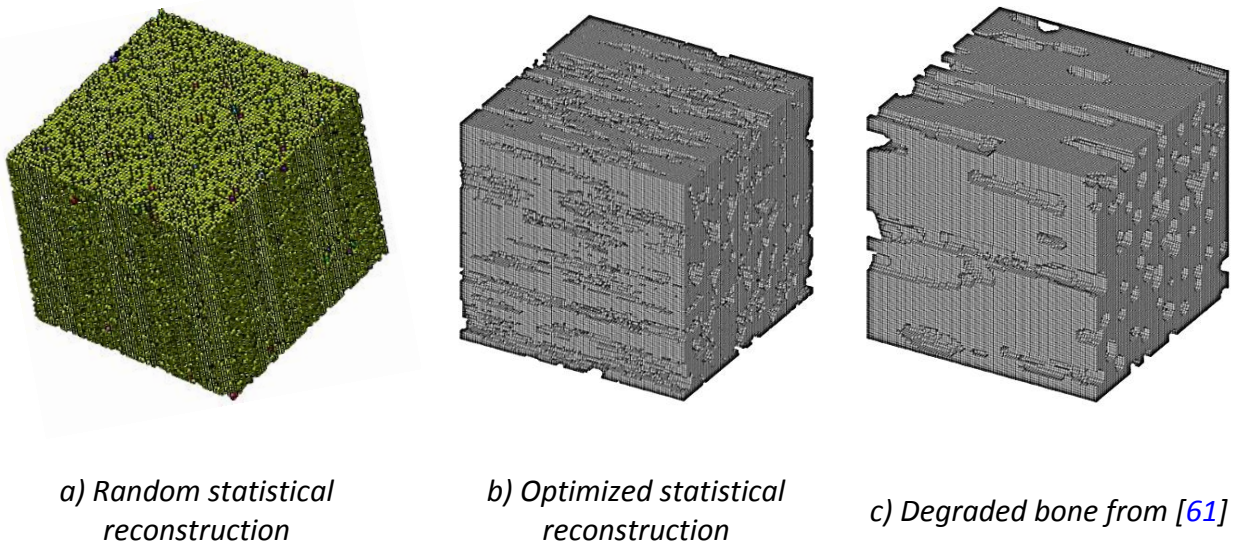


Figure 6: Matrix with 100*100*100 voxels having 63% volume fraction

The reconstructed models and the degraded model with their corresponding volume fraction are presented in [Figure 7](#) for different volume fractions 84%, 73%, and 63%.

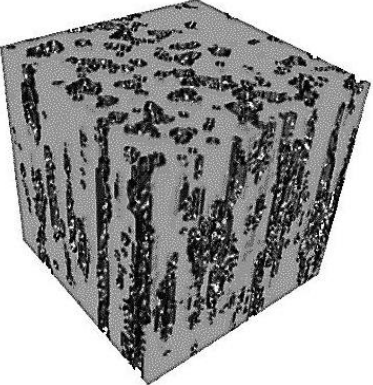
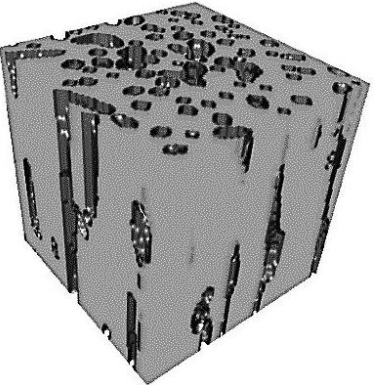
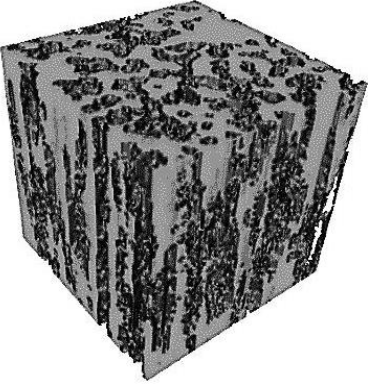
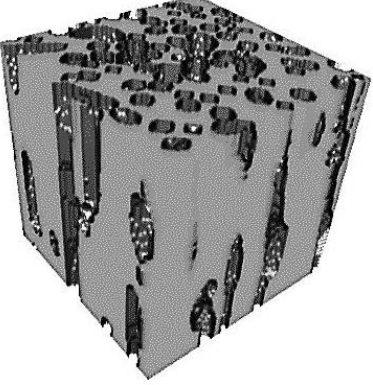
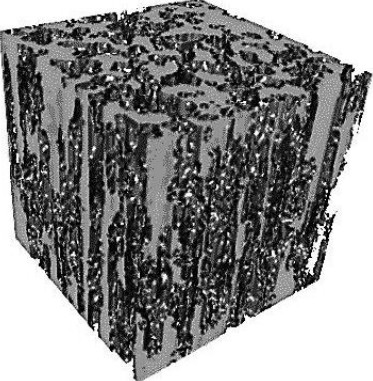
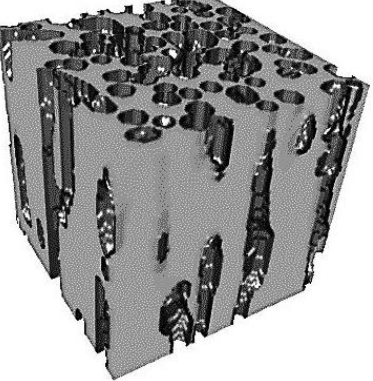
Vol. fraction	Statistical	Degraded from [61]
84%		
73%		
63%		

Figure 7: Left- Statically reconstructed microstructures, Right- Degraded microstructures from [61].

3.2 Mechanical characterization

Young modulus, strains, and stresses in the main directions x, y, and z, are obtained by using the Finite Element Method, ABAQUS CAE software. For each voxel, the elastic modulus is derived as a function of the local voxel bone density. We extracted macroscopic Hooke's Law from averaging the overall sample. The results for the load in the x-direction are presented in [Figure 8](#).

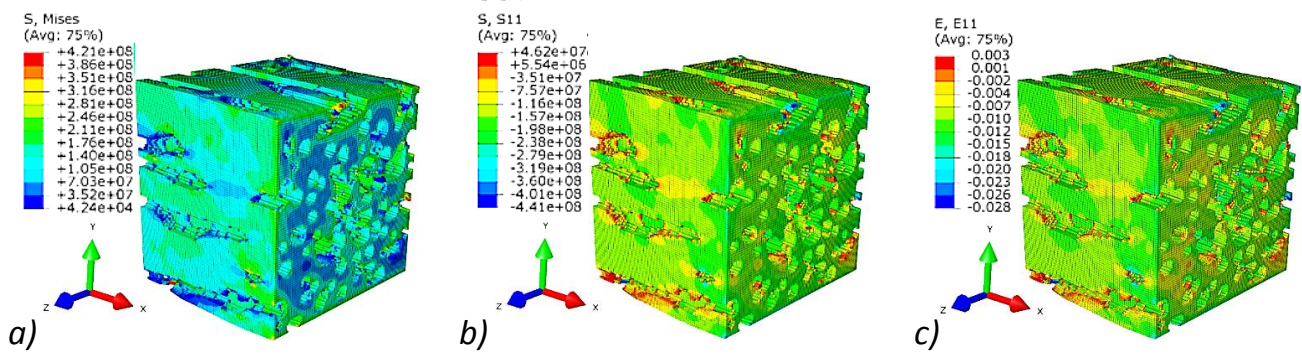


Figure 8: Stresses (in Pa) and strains in the degraded bone with a 63% volume fraction in the x-direction; a) Von Mises Stress; b) Stress in x-direction; c) Strains in x-direction.

Two other optimized statistical bone microstructures were reconstructed with 73% and 84% volume fractions. Homogenized macroscopic stiffness coefficients (i.e. Young modulus) were extracted for the validation of the reconstruction process, assuming the material (solid bone phase) mechanical behavior was linear elastic with a Young modulus $E = 15$ GPa (average value for cortical bone) and Poisson's ratio is 0.3.

The degraded model presented values of Young modulus between 8.53 GPa and 14.5 GPa. Values obtained from the reconstructed microstructures varied between 9.85 GPa and 15.5 GPa. The errors developed from the microstructures variations for the Young modulus varied from 10% for the maximum Young modulus of 15.5 GPa up to a value of 14% for a Young modulus of 12.4 GPa. Results are reported in [Table 2](#).

Volume Fraction		Young Modulus (GPa)	Error (%)
93% initial		14.5	-
84%	Degraded	13.8	-
	Reconstructed	15.5	+10
73%	Degraded	10.6	-
	Reconstructed	12.4	+14
63%	Degraded	8.53	-
	Reconstructed	9.85	+13
60%	Degraded	7.79	-

Table 2: Modulus of elasticity in specific directions for the degraded and statistical bone microstructures.

4. Discussion

The comparison of the obtained TPCFs values in the three directions x, y and z ([Figure 5](#)) shows good correlation with two directions being almost identical (y and z) and one close (x). This means that the proposed statistical reconstruction method was able to provide very similar microstructure distribution as compared to the reference case. This is validated by the error value on the beta coefficient in [Table 1](#). For an initial volume fraction of 93% down to 73% degradation, the error remains small (under 1%). When porosity increases (volume fraction of 63%), the error has increased up to 1.7%. We can observe

this effect on the distributed microstructure of [Figure 6](#). The constructed model contains connections, holes, and fossae similarly to the real bone, but the morphology is different. This will of course influence the structural evolution in time. Since cells biological response is highly dependent on the local bone microstructure distribution and the corresponding local mechanical forces applied to this local microstructure, the local bone density evolution will be impacted. However, the two proposed methodologies (being phase degradation [61] or statistical reconstruction) are unable to provide an exact match with the real bone microstructure degradation as both degradation scenarii are different from real bone. Hence, variations will develop between the different cases. Nevertheless, these variations remain small as presented in the results section, but as the microstructure distribution has a large impact on the bone mechanobiology (as per the patient dependency aspects), this remains to be studied more deeply at a later stage. Nonetheless, the geometry of the optimized matrix ([Figure 6b](#)) resembles the degraded bone ([Figure 6c](#)). By considering TPCFs of the degraded bone model ([Figure 6c](#)) and the random one ([Figure 6a](#)), the error is 8.68% which is about five times bigger than compared to the reconstructed one ([Figure 6b](#)). We can assess here that when comparing the random statistical distribution with the reference case, an error as small as 8.68% is already large for a proper mechanobiological modeling (even at the continuous macroscopic scale). Hence, obtaining the proper microstructure remains a desirable objective. For the optimized statistical reconstruction at 63% volume fraction of [Figure 6b](#) and [Figure 6c](#), we obtained an error of 1.74%. This enabled to have a much closer distribution to the reference case. The degraded, reconstructed and random models are all percolated in all directions and the difference is mainly related to the difference in their morphology. With lower volume fraction, the error would continue to increase with their percolation connections.

The observation is made on [Figure 7](#) that higher volume fraction enables better reconstruction results and as the volume fraction decreases, the error increases proportionally. For the hereby proposed method, to improve the model precision, we could use smaller values of β intervals by step of 0.1 during analyses to find better optimized microstructure. As the porosity increases with decreasing volume fraction for each proposed method (statistical and degraded), this porosity remains heterogeneously distributed. In fine, both methods are not completely adequate to model the bone degradation. Although the degradation method resembles better the bone structure, it degrades the bone in a homogeneous manner everywhere on the solid bone surface leaving solid bone islands which are not biologically realistic. On the other hand, the statistical bone structure has better compatible physical characteristics compared to real bone, but without a proper microstructure distribution. Again, bone remodeling is cell biology driven, and since cells activity depends on their physical environment, the local bone microstructure distribution influences specifically the bone degradation evolution. The exact mechanobiological coupling between cell activity and local bone microstructure distribution being to this day unknown, it is not possible to foresee which is the best proposed model ; the degradation model having a closer bone like microstructure but with a poorer degradation process, or the statistical model having a less bone like distribution but with better mechanical characteristics. However, since most predictive numerical bone remodeling model are mechanically driven at the meso and macro scale, we observe that the statistical model would respond better to this input. This effect needs to be investigated further.

The results of effective mechanical properties show, as expected, a decrease in Young's modulus with a decrease in volume fraction. Noticeably, the error in the stiffness evaluation is variable for the different cases, but it remains reasonably small and shows good quality of the reconstruction procedure

even when the volume fraction is decreasing. This tends to show from the mechanobiological point of view that developing a predictive macroscopic model based only on equivalent stiffness is far from being enough. This shows that with equivalent stiffness, the bone microstructure distribution can be very different. Nonetheless, all reconstructed cases show a higher stiffness than the original cases. This may be due to the concentration distribution of the voxels in the x-direction, as the reconstruction procedure shows variability with the exact degraded microstructures. This needs to be investigated at a later stage

5. Conclusion

An initial bone microstructure was obtained from high-resolution X-ray computed tomography images. The osteoporotic evolution was simulated from a degradation model based on existing literature and several degraded microstructures were extracted at different times with different volume fractions. We used statistical reconstruction to find optimum microstructures that correspond to the degraded scenario and evaluated the usefulness of the microstructure distribution influence from an optimized coefficient beta that can provide various microstructure distributions at a given volume fraction. By interpolating between the time evolutions, the Young's modulus and Poisson ratio of any intermediate volume fractions were obtained. This can be related, but not solely as it also depends on the microstructure distribution, to the patient dependent osteoporosis evolution as measured by standard bone density measurements. Future works include integrating two-point correlation cluster function to improve the accuracy of the statistical interpolation for quality of the bone microstructure reconstruction and the study of the relationship between reconstructed microstructure and beta parameter.

Acknowledgment

The authors would like to thank Dr. Martine Pithioux from Science and Mouvement Institute, Université Aix-Marseille and Timone Hospital in France for providing the real bone sample from which this work was carried out. The work was supported by the Center for International Scientific Studies & Collaboration (CISSC), Ministry of Science, Research & Technology of Iran, as well as the French Embassy in Iran through Campus France and PHC Gundishapur Program.

References

- [1] Hardy, R. and Cooper M. (2009). Bone loss in inflammatory disorders. *Journal of Endocrinology* 201(3): 309-320.
- [2] Sugawara, Y., et al. (2005). Three-dimensional reconstruction of chick calvarial osteocytes and their cell processes using confocal microscopy. *Bone* 36(5): 877-883.
- [3] Hadjidakis, D. J. and Androulakis, I.I. (2006). Bone remodeling. *Annals of the New York Academy of Sciences* 1092(1): 385-396.
- [4] Klein-Nulend, J., et al. (2013). Mechanosensation and transduction in osteocytes. *Bone* 54(2): 182-190.

- [5] Florencio-Silva, R., et al. (2015). Biology of bone tissue: structure, function, and factors that influence bone cells. *BioMedical research international*, 2015: 421746.
- [6] Veni, M.A.C. and Rajathi P. (2017). Interaction between bone cells in bone remodeling. *Journal of Academic Dental Education*, 2: 1-6.
- [7] Stoltz J-F., et al. (2018). Influence of mechanical forces on bone: introduction to mechanobiology and mechanical adaptation concept. *Journal of Cellulo Immunotherapy*, 4: 10-12.
- [8] Stoltz J-F., et al. (2019). Response of bone cells to mechanical stimulations: an overview, IOS Press, *Biomedical Health and Research, Stem Cells and Regenerative Medicine*, 79: 71-76.
- [9] Wang, Q. and Seeman E. (2008). Skeletal growth and peak bone strength. *Best Practice & Research Clinical Endocrinology & Metabolism*, 22(5): 687-700.
- [10] Thudium, C. (2014). Development of novel models for studying osteoclasts, Lund University Faculty of Medicine Doctoral dissertation, 2014:111.
- [11] Bakalova, L., et al. (2018). Intracortical Bone Mechanics Are Related to Pore Morphology and Remodeling in Human Bone. *Journal of Bone Mineral Research*, 33(12): 2177-2185.
- [12] Ramachandran, R. (2006). Hierarchy of bone structure report. *Complex Polymer Morphology*, College of Engineering and Applied Science, University of Cincinnati, https://www.eng.uc.edu/~beaucag/Classes/MorphologyofComplexMaterials/Hierarchy_of_Bone_Structure.pdf
- [13] Lang, T. F., et al. (2006). Adaptation of the proximal femur to skeletal reloading after long-duration spaceflight. *Journal of Bone and Mineral Research* 21(8): 1224-1230.
- [14] Chen, H., et al. (2013). Age-related changes in trabecular and cortical bone microstructure. *International journal of endocrinology*, 2013:213234.
- [15] Carter, D., et al. (1996). Mechanical factors in bone growth and development. *Bone* 18(1): S5-S10.
- [16] Casanova, R., et al. (2010). Temporal evolution of skeletal regenerated tissue: what can mechanical investigation add to biological? *Medical & biological engineering & computing* 48(8): 811-819.
- [17] Huijkes, R., et al. (2000). Effects of mechanical forces on maintenance and adaptation of form in trabecular bone. *Nature* 405(6787): 704-706.
- [18] Wolff, Y. (1892). *Das Gesetz der Transformation der Knochen*. Berlin: Verlag von August Hirschwald.
- [19] Cowin, S.C. (1986). Wolff's law of trabecular architecture at remodeling equilibrium. *Journal of Biomedical Engineering*, 108(1):83-88.
- [20] Frost, H.M. (1987). Bone "mass" and the "mechanostat": a proposal. *The anatomical record* 219(1): 1-9.
- [21] Giorgio, I. et al. (2020). In-depth gaze at the astonishing mechanical behavior of bone: A review for designing bio-inspired hierarchical metamaterials, *Mathematics and Mechanics of Solids*, 26(7): 1074-1103.
- [22] Pivonka, P., et al. (2008). Model structure and control of bone remodeling: a theoretical study. *Bone* 43(2): 249-263.
- [23] Scala, I., et al. (2017). Mechanically-driven bone remodeling simulation: Application to LIPUS treated rat calvarial defects. *Mathematics and Mechanics of Solids* 22(10): 1976-1988.
- [24] Madeo, A., et al. (2012). A second gradient continuum model accounting for some effects of micro-structure on reconstructed bone remodeling. *Comptes Rendus Mécanique* 340(8): 575-589.
- [25] Giorgio, I., et al. (2019). On mechanically driven biological stimulus for bone remodeling as a diffusive phenomenon, *Biomechanics and Modelling in Mechanobiology*, 18(3): 1639-1663.

- [26] Scerrato, D., Bersani, A., Giorgio, I. (2021). Bio-Inspired Design of a Porous Resorbable Scaffold for Bone Reconstruction: A Preliminary Study, *Biomimetics*, 6(1), 18.
- [27] I. Giorgio, U. Andreaus, F. Dell’Isola, T. Lekszycki, Viscous second gradient porous material for bones reconstructed with bio-resorbable grafts, *Extreme Mechanics Letters*, 2017, 13, 141-147
- [28] F. Dell’Isola, V.A. Eremeyev, A.V. Porubov, Advances in Mechanics of microstructured media and structures, *Advanced Structured Materials*, 2018, 87, ISBN 978-3-319-73694-5
- [29] I. Giorgio, M. De Angelo, E. Turco, A. Misra, A Biot–Cosserat two-dimensional elastic nonlinear model for a micromorphic medium, *Continuum Mechanics and Thermodynamics*, 2020, 32(5), 1357-1369.
- [30] G. La Valle, S. Massoumi, A new deformation measure for micropolar plates subjected to in-plane loads, *Continuum Mechanics and Thermodynamics*, 2022, 34(1), 243-257.
- [31] Hegedus, D. and Cowin, S. (1976). Bone remodeling II: small strain adaptive elasticity. *Journal of elasticity* 6(4): 337-352.
- [32] Andreaus, U., et al. (2011). Optimal-tuning PID control of adaptive materials for structural efficiency. *Structural and Multidisciplinary Optimization* 43(1): 43-59.
- [33] Prendergast, P. and Taylor, D. (1994). Prediction of bone adaptation using damage accumulation. *Journal of biomechanics* 27(8): 1067-1076.
- [34] Doblaré, M. and García, J. (2002). Anisotropic bone remodeling model based on a continuum damage-repair theory. *Journal of biomechanics* 35(1): 1-17.
- [35] Dell’Isola, F., et al. (2015). At the origins and in the vanguard of peridynamics, non-local and higher-gradient continuum mechanics: an underestimated and still topical contribution of Gabrio Piola. *Mathematics and Mechanics of Solids* 20(8): 887-928.
- [36] Misra, A. and Poorsolhjouy, P. (2015). Identification of higher-order elastic constants for grain assemblies based upon granular micromechanics. *Mathematics and Mechanics of Complex Systems* 3(3): 285-308.
- [37] Placidi, L., et al. (2015). Gedanken experiments for the determination of two-dimensional linear second gradient elasticity coefficients. *Zeitschrift für angewandte Mathematik und Physik* 66(6): 3699-3725.
- [38] Abali, B. E., et al. (2017). Theory and computation of higher gradient elasticity theories based on action principles. *Archive of Applied Mechanics* 87(9): 1495-1510.
- [39] Dell’Isola, F., et al. (2017). Higher-gradient continua: The legacy of Piola, Mindlin, Sedov and Toupin and some future research perspectives. *Mathematics and Mechanics of Solids* 22(4): 852-872.
- [40] Rémond, Y., et al. (2016). Applied RVE reconstruction and homogenization of heterogeneous materials, Wiley Online Library.
- [41] Martin, M., et al. (2017). A thermodynamically consistent model of bone rotary remodeling: a 2D study. *Computer methods in biomechanics and biomedical engineering* 20(sup1): 127-128.
- [42] George, D., et al. (2017). Examples of multiscale and multiphysics numerical modeling of biological tissues. *Bio-medical materials and engineering* 28(s1): S15-S27.
- [43] Spingarn, C., et al. (2017). Multiphysics of bone remodeling: a 2D mesoscale activation simulation. *Bio-medical materials and engineering* 28(s1): S153-S158.
- [44] Kazempour, M., et al. (2019). Homogenization of heterogeneous brain tissue under quasi-static loading: a visco-hyperelastic model of a 3D RVE. *Biomechanics and modeling in Mechanobiology* 18(4): 969-981.
- [45] Hashemi, M. S., et al. (2020). A novel machine learning based computational framework for homogenization of heterogeneous soft materials: application to liver tissue. *Biomechanics and modeling in Mechanobiology*, 19: 1131-1142.

- [46] Hollister, S.J., et al. (1994). A homogenization sampling procedure for calculating trabecular bone effective stiffness and tissue level stress. *Journal of biomechanics* 27(4): 433-444.
- [47] Tsubota, K-I., et al. (2009). Computer simulation of trabecular remodeling in human proximal femur using large-scale voxel FE models: Approach to understanding Wolff's law. *Journal of biomechanics* 42(8): 1088-1094.
- [48] Jang, I. G. and Kim, I.Y. (2010). Computational simulation of simultaneous cortical and trabecular bone change in human proximal femur during bone remodeling. *Journal of biomechanics* 43(2): 294-301.
- [49] Marzban, A., et al. (2015). Numerical simulation of load-induced bone structural remodeling using stress-limit criterion. *Computer methods in biomechanics and biomedical engineering*, 18(3): 259-268.
- [50] Kersh, M. E., et al. (2013). Measurement of structural anisotropy in femoral trabecular bone using clinical-resolution CT images. *Journal of biomechanics* 46(15): 2659-2666.
- [51] Lian, W.-D., et al. (2013). Image-based computational homogenization and localization: comparison between X-FEM/levelset and voxel-based approaches. *Computational Mechanics* 51(3): 279-293.
- [52] Kazempour, M., et al., (2019). Numerical simulation of osteoporosis degradation at local scale : a preliminary study on the kinematic loss of mechanical bone stiffness. *Stem Cells and Regenerative Medicine*, IOS Press, 87-94.
- [53] George, D., et al. (2018). A multiphysics stimulus for continuum mechanics bone remodeling. *Mathematics and Mechanics of Complex Systems* 6(4): 307-319.
- [54] George, D., et al. (2019). Integrating molecular and cellular kinetics into a coupled continuum mechanobiological stimulus for bone reconstruction. *Continuum Mechanics and Thermodynamics* 31(3): 725-740.
- [55] George, D., et al. (2020). A new comprehensive approach for bone remodeling under medium and high mechanical load based on cellular activity. *Mathematics and Mechanics of Complex Systems*, 8(4): 287-306.
- [56] Goda, I., et al. (2012). A micropolar anisotropic constitutive model of cancellous bone from discrete homogenization. *Journal of the mechanical behavior of biomedical materials*, 16: 87-108.
- [57] R ath, C., et al. (2013). Scaling relations between trabecular bone volume fraction and microstructure at different skeletal sites. *Bone* 57(2): 377-383.
- [58] Goda, I., et al. (2014). A 3D elastic micropolar model of vertebral trabecular bone from lattice homogenization of the bone microstructure. *Biomechanics and modeling in Mechanobiology* 13(1): 53-83.
- [59] Wierszycki, M., et al. (2014). A two-scale approach for trabecular bone microstructure modeling based on computational homogenization procedure. *Computational Mechanics* 54(2): 287-298.
- [60] Goda, I., et al. (2016). Optimal internal architectures of femoral bone based on relaxation by homogenization and isotropic material design. *Mechanics Research Communications* 76: 64-71.
- [61] Bagherian, A., et al. (2019). A novel numerical model for the prediction of patient-dependent bone density loss in microgravity based on micro-CT images. *Continuum Mechanics and Thermodynamics* 32:927-943.
- [62] Sheidaei, A., et al. (2019). Influence of bone microstructure distribution on developed mechanical energy for bone remodeling using a statistical reconstruction method. *Mathematics and Mechanics of Solids* 24(10): 3027-3041.
- [63] Famouri, S., et al. (2020). Refining anticipation of degraded bone microstructures during osteoporosis based on statistical homogenized reconstruction method via quality of connection function. *International Journal of Computational Materials Science and Engineering*: 9(4): 2050023.

- [64] Hashin, Z. and Shtrikman S. (1963). A variational approach to the theory of the elastic behaviour of multiphase materials. *Journal of the Mechanics and Physics of Solids* 11(2): 127-140.
- [65] Gokhale, A., et al. (2005). Constraints on microstructural two-point correlation functions. *Scripta Materialia* 53(8): 989-993.
- [66] Adams, B. L., et al. (2012). *Microstructure sensitive design for performance optimization*, Butterworth-Heinemann.
- [67] Fullwood, D., et al. (2008). Gradient-based microstructure reconstructions from distributions using fast Fourier transforms. *Materials Science and Engineering: A* 494(1-2): 68-72.
- [68] Gerchberg, R. W. (1972). A practical algorithm for the determination of phase from image and diffraction plane pictures. *Optik* 35: 237-246.